10.1071/CH20288_AC



Australian Journal of Chemistry 2021, 74(4), 282-289

# Supplementary Material

## Self-Assembly of CDs@$NH_2$-MOF(Ni)/n-$Bu_4NBr$ and its Catalytic Performance for $CO_2$ Fixation with Epoxides

*Kai Huang*[A,B] *and Xiaomeng Zhang*[A]

[A]School of Chemistry and Chemical Engineering, Southeast University, Jiangning District, Nanjing 211189, China.
[B]Corresponding author. Email: huangk@seu.edu.cn

## 1. Materials and Methods

### 1.1. Materials

All reagents and solvents were purchased and used without further purification. Analytical reagent grade nickel acetate tetrahydrate ($C_4H_6NiO_4 \cdot 4H_2O$, AR), urea ($H_2NCONH_2$, AR), citric acid monohydrate ($C_6H_8O_7 \cdot H_2O$, AR), and 2-aminoterephthalic acid ($NH_2$-BDC, AR) were obtained from Sinopharm Chemical Regent Co. Ltd (China). N, N-dimethylformamide (DMF, AR), absolute ethanol ($C_2H_5OH$, AR), deionized water, hydrofluoric acid (HF, AR), were purchased from Shanghai Macklin Biochemical Co. Ltd (China).

### 1.2. Synthetic Methods

The preparation method of CDs@$NH_2$-MOF is shown in Scheme 1.

### 1.3. Synthesis of CDs, $NH_2$-MOF(Ni) and CDs@$NH_2$-MOF(Ni)

Synthesis method of the CDs can be obtained from reference. [39] Synthesis method of $NH_2$-MOF(Ni) and CDs@$NH_2$-MOF(Ni) would be in detail. To nickel acetate tetrahydrate (1 mmol, 0.2488 g), 2-aminoterephthalic acid ($NH_2$-BDC) (2 mmol, 0.3323 g), 20 mL distilled water was added 1 mL Hydrofluoric acid was added drop-wise under agitation. Then the solution was transferred to 50 mL Teflon-lined stainless-steel autoclave and heated at 220 °C for 8 h. When cooled to 25 °C, a green solid precipitate was obtained and washed severally with ethanol. Next, a green solid precipitate was added to a 100 mL beaker containing 25 mL of N, N-dimethylformamide and stirred for 10 min. After filtering, a green solid precipitate was put into a 100 mL round bottom flask containing 25 mL of absolute ethanol and reacted at 80 °C for 12 h. [41] Finally, the filtered product was dried in a vacuum oven at 80 °C for 12 h. Then the $NH_2$-MOF(Ni) was obtained. Synthesis of CDs@$NH_2$-MOF(Ni) just change the first step of condition, which adds 500 mg of CDs to the raw material.

### 1.4. Methods of Material Characterization

Powder X-ray diffraction (XRD) patterns were obtained to identify the structures of the prepared catalysts using an Ultima IV X-ray diffractometer with Cu Kα radiation (λ = 0.154 06 nm). The surface morphologies of the catalysts were observed using scanning electron microscopy (SEM, TESCAN 5136 MM). Compositional analysis of the sample was obtained by Energy dispersive X-Ray (EDX). Transmission electron microscopy (TEM) profiles were obtained using a FEI Tecnai G2 F20 electron microscope with an accelerating voltage of 200 kV. Thermal Gravimetry (TG) of the synthesized samples was measured on the Pyris Diamond of Perkin-Elmer to analyze the thermal behavior. The BET surface area and total pore volume were measured using a Micromeritics ASAP 2020 Plus 1.03 apparatus. Fourier transform infrared (FT-IR) profiles of the prepared catalysts were recorded using a Thermo Fisher Nicolet 5700 spectrophotometer in the range of 400-2000 $cm^{-1}$.

### 1.5. Detailed explanation of the mechanism of the catalyst

In detail, the amine group of catalyst CDs@$NH_2$-MOF(Ni) acts first on the oxygen atom of $CO_2$ to activate $CO_2$, and the oxygen atom of PO is also acted upon by the Lewis acid site ($Ni^{2+}$) of the catalyst CDs@$NH_2$-MOF(Ni). Meanwhile, a large amount of bromide ions of co-catalyst TBAB attack PO with less hindered β-carbon

atom to open the PO. Then, the oxygen atom of the polarized carbon dioxide molecule attacks the β-carbon atom of the ring-opened epoxide, and the activated oxygen atom of PO attacks the carbon atom of $CO_2$. Next, catalyst CDs@$NH_2$-MOF(Ni) and bromide ions are eliminated to produce an intermediate, which is the β-carbon atoms of PO combined with the oxygen atom of $CO_2$ to form a single bond C-O, and the oxygen atom of PO combined with the carbon atom of $CO_2$ to form a single bond O-C. Finally, PC will be produced, and free bromide ions and catalyst CDs@$NH_2$-MOF(Ni) will also enter the next cycle. From the FT-IR (Figure 2) of the carbon dots, it can be clearly seen that the surface of the carbon dots contains a large number of amine groups, and the doping of the carbon dots increases the specific surface area (Figure 6). Combining the mechanism diagram, we can clearly see that the carbon dots expand the number of amine groups and increase the local reaction space, so the conversion rate of CDs@$NH_2$-MOF(Ni)/TBAB is 16% higher than that of $NH_2$-MOF(Ni)/TBAB.

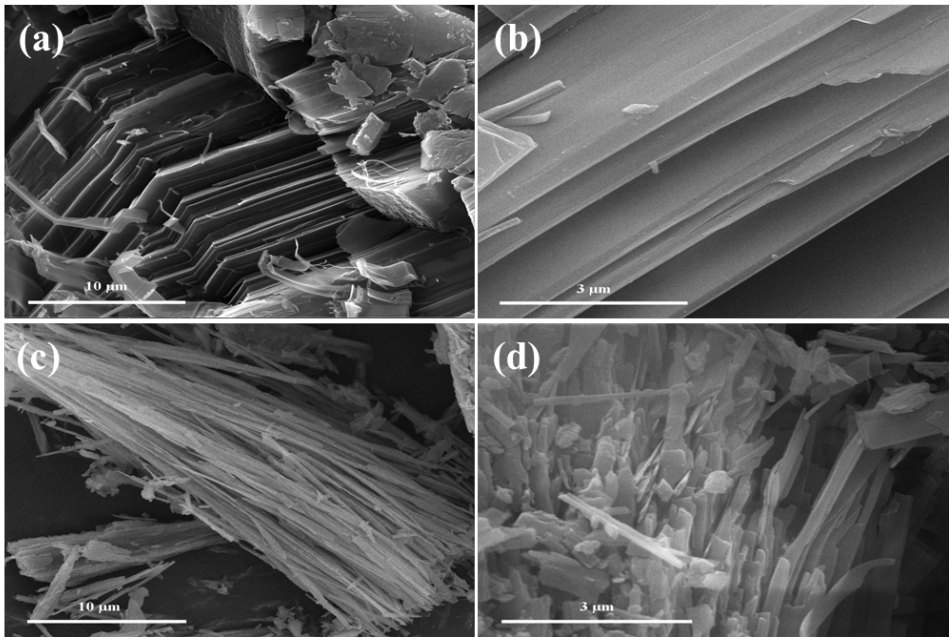


Figure S1. SEM images of (a), (b) $NH_2$-MOF(Ni) and (c), (d) CDs@$NH_2$-MOF(Ni).

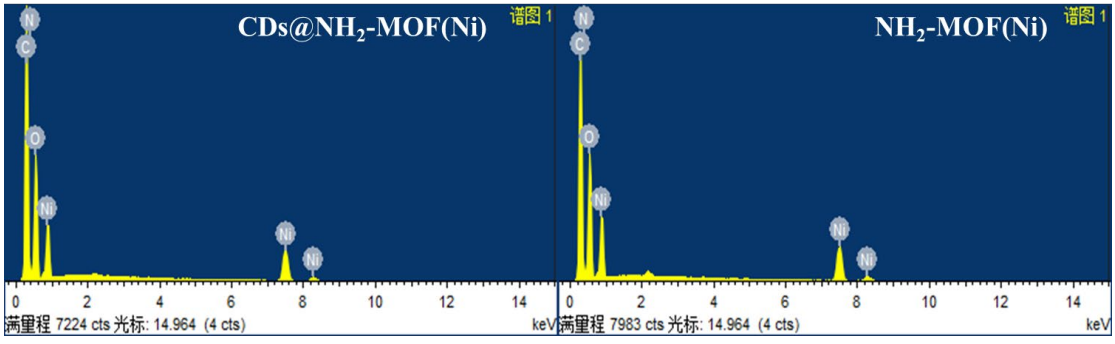


**Figure S2.** The energy dispersive spectrum (EDS) of CDs@$NH_2$-MOF(Ni) and $NH_2$-MOF(Ni)

Compositional analysis reveals the presence of C, O, N, and Ni elements in two samples. The presence of C, O, N, and Ni (three positions) at 0.2 kev, 0.4 kev, 0.6 kev and 0.8 kev, 7.4 kev, 8.2 kev, respectively, were confirmed by EDX results .

**Table S1** Atomic ratios of C, N, O, Ni in EDX results of CDs@$NH_2$-MOF(Ni) and $NH_2$-MOF(Ni).

| Atomic Percentage | C (%) | N (%) | O (%) | Ni (%) |
|---|---|---|---|---|
| $NH_2$-MOF(Ni) | 53.25 | 8.41 | 33.43 | 4.91 |
| CDs@$NH_2$-MOF(Ni) | 54.46 | 9.46 | 32.73 | 3.35 |

**Table S2.** Cycloaddition of propylene oxide and $CO_2$ using various catalysts.

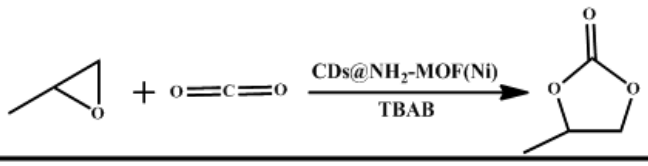


| Entry | Catalyst | Temperature (℃) | Conversion (%) | Selectivity (%) | Yield (%) |
|---|---|---|---|---|---|
| 1 | None | 130 | 0 | 0 | 0 |
| 2 | $C_4H_6NiO_4·4H_2O$ | 130 | Trace | — | — |
| 3 | TBAB | 130 | 43 | 97 | — |
| 4 | CDs | 130 | Trace | 0 | 0 |
| 5 | $NH_2$-BDC | 130 | — | — | — |
| 6 | $NH_2$-MOF(Ni) | 130 | 28 | 71 | 19 |
| 7 | CDs@$NH_2$-MOF(Ni) | 130 | 32 | 79 | 23 |
| 8 | TBAB/ $NH_2$-MOF(Ni) | 130 | 81 | 99 | 80 |
| 9 | TBAB/CDs@$NH_2$-MOF(Ni) | 130 | 97 | 99 | 96 |

Conditions PO: 100 mmol, $CO_2$ (2.2MPa), 130℃, 7 h.

In the absence of any catalyst and co-catalyst TBAB (Entry 1), no product PC was detected. Meanwhile, no product PC was detected in the presence of $C_4H_6NiO_4·4H_2O$, CDs, and $NH_2$-BDC without TBAB (Entry 2, 4, 5). When a nucleophilic co-catalyst tetrabutylammonium bromide (TBAB) was selected as the catalyst alone (Entry 3), only 43% conversion of PO and 97% selectivity of PC were shown. In the absence of TBAB, the original catalyst $NH_2$-MOF(Ni) and CDs@$NH_2$-MOF(Ni) gave only 28% and 32% PO conversion, with 71% and 79% PC selectivity, respectively (Entry 6, 7). Fortunately, higher conversion and selectivity were obtained when the catalyst and co-catalyst acted as a synergistic catalytic system. As shown in Entry 8-9, 81% and 97% PO conversion and 97% and 99% PC selectivity were obtained, respectively. Evidently, catalysts $NH_2$-MOF(Ni) and CDs@$NH_2$-MOF(Ni) have better catalytic effects than the previous materials, while the conversion of catalyst CDs@$NH_2$-MOF(Ni), 16% higher

than that of $NH_2$-MOF(Ni), is due to the action of CDs.

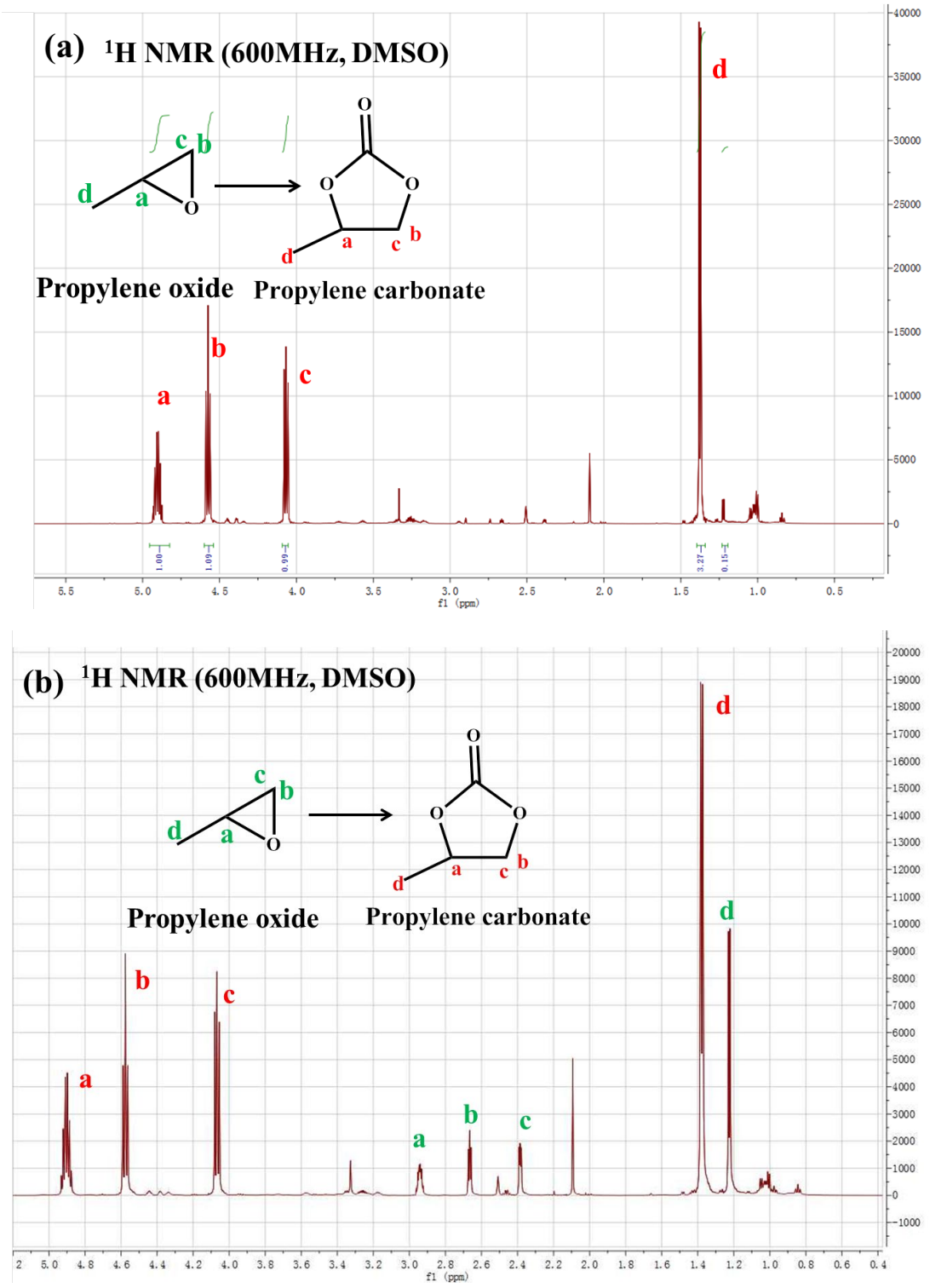


**Figure S3.** The $^1$H-NMR spectrum of the Propylene oxide and the Propylene carbonate, (a) results of catalyst system CDs@$NH_2$-MOF(Ni)/TBAB, (b) results of catalyst system $NH_2$-MOF(Ni)/TBAB

As shown in Figure S3, the styrene oxide of catalyst system

CDs@$NH_2$-MOF(Ni)/TBAB is almost completely reacted while the catalyst system $NH_2$-MOF(Ni)/TBAB has a small amount remaining.

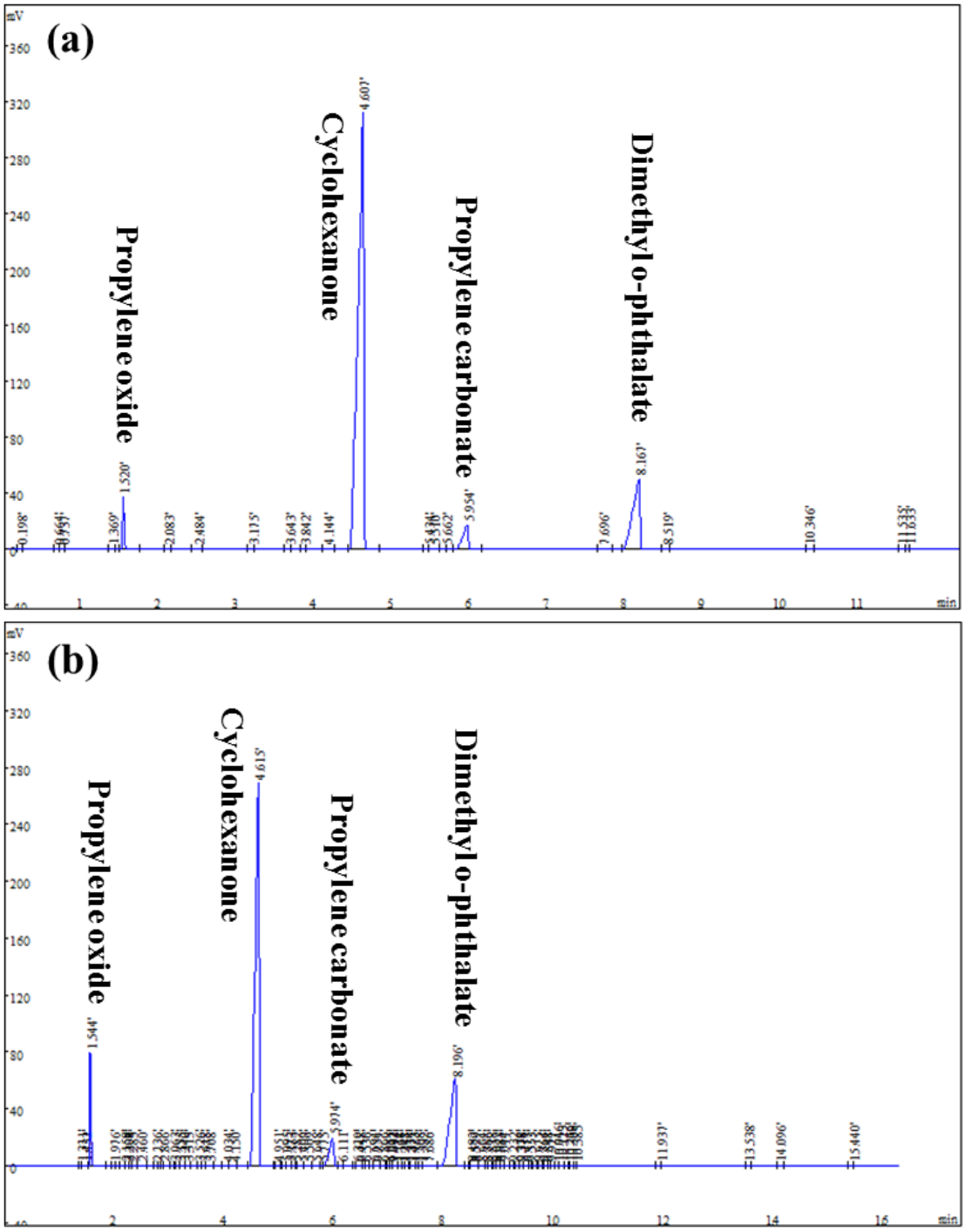


**Figure S4.** The GC results: (a) catalyst system CDs@$NH_2$-MOF(Ni)/TBAB, (b) catalyst system $NH_2$-MOF(Ni)/TBAB

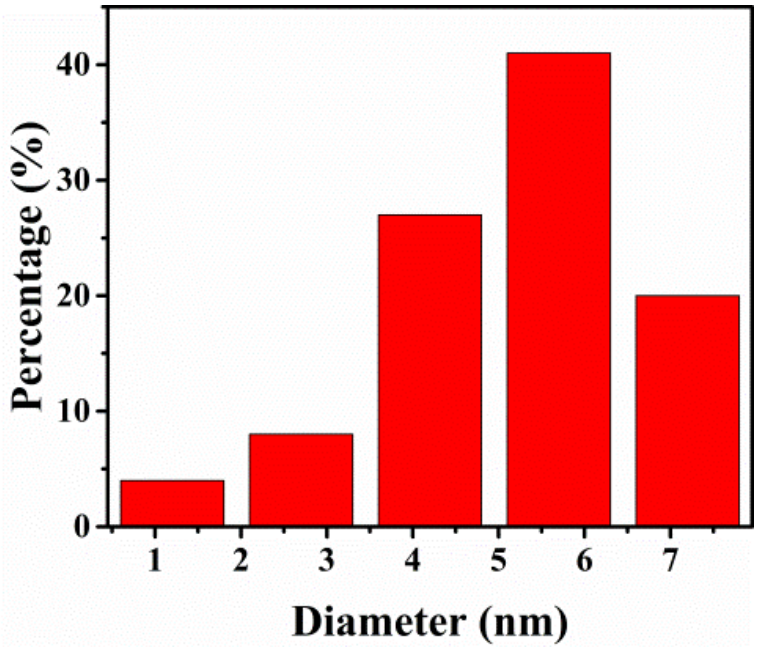


Figure S5. Particle size distribution of as-prepared CDs

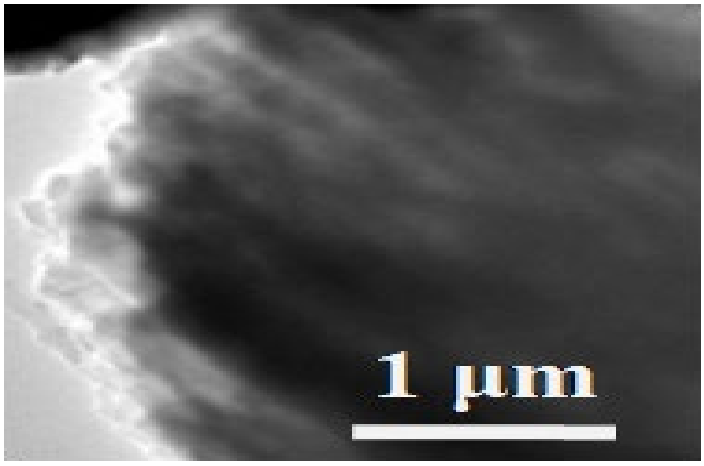


Figure S6. TEM image of the catalyst after five catalytic cycles

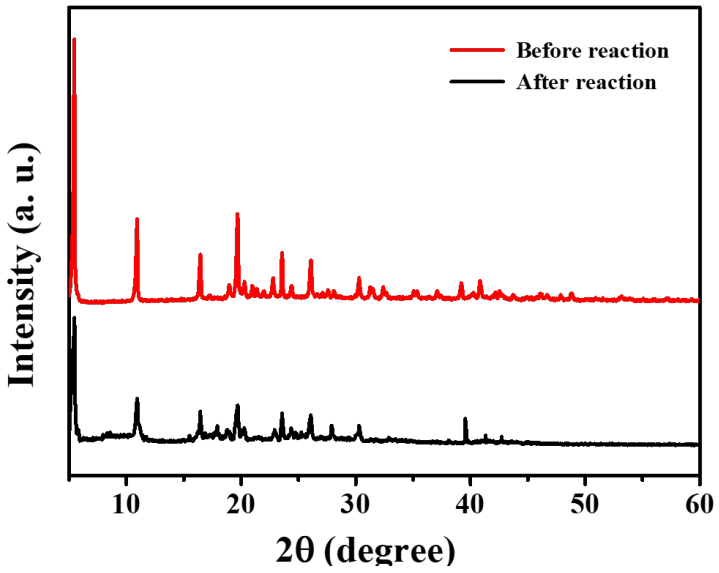


Figure S7. XRD image of the catalyst after five catalytic cycles

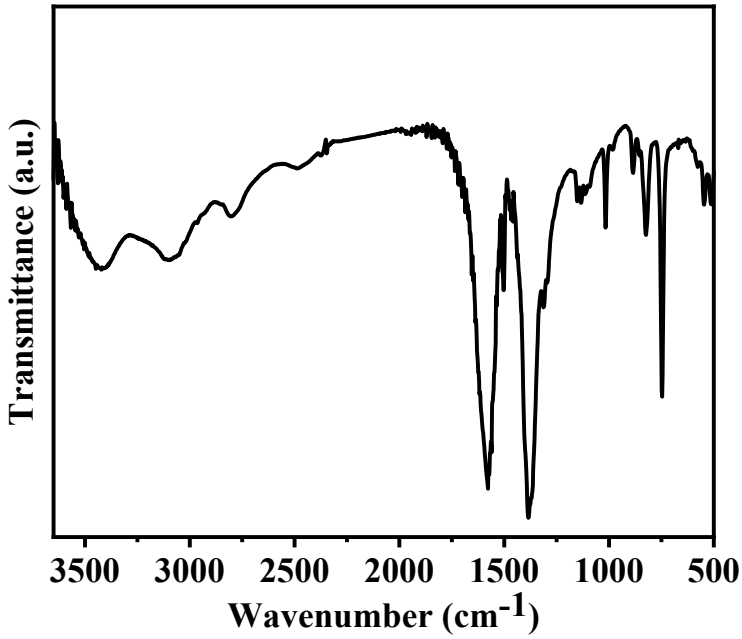


Figure S8. IR image of the catalyst after five catalytic cycles

From figure S7 S8, we can clearly see that the catalyst recovered by multiple cycles has slightly changed, but the general characteristic peaks have not changed. Such as: the characteristic peak of carbon nanodots in XRD and the characteristic peak of amine groups in IR. Simultaneously, the TEM image of the catalyst after multiple cycles also shows its good structural stability (Figure S6).

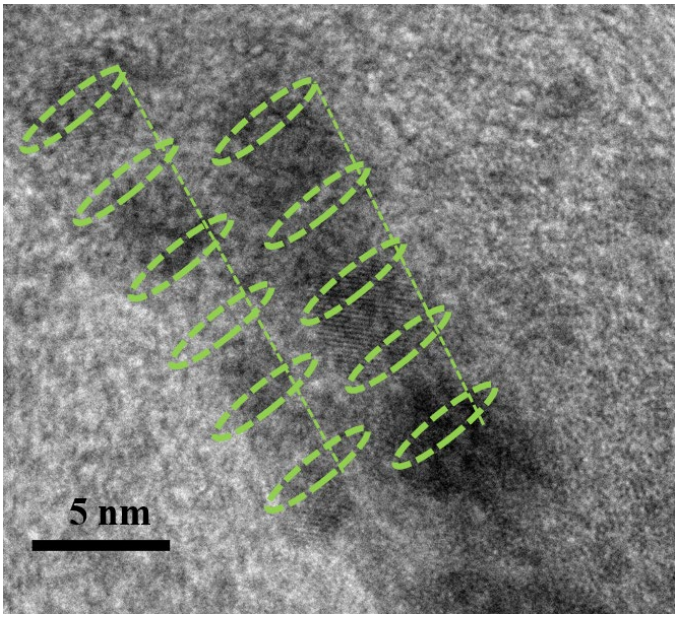


Figure S9. HRTEM image of the CDs@$NH_2$-MOFs

SEM and TEM test results also show that carbon dots enter the new material and play a role in the construction of material CDs@$NH_2$-MOFs. To further illustrate this point, we took a high magnification TEM picture again. From figure S9 we can see the regularly arranged carbon dots in material CDs@$NH_2$-MOF(Ni). This is in line with our expected results.